JAST, Vol. 2, No. 3, pp 1–8

JAST
Journal of Aerospace Science and Technology

Transonic Turbulent Flow Computations on Unstructured Triangular Grids

M.T. Manzari[1]

The numerical simulation of 2D steady transonic turbulent flow over aerofoil sections is considered on unstructured triangular grids. The mass-averaged Navier-Stokes equations are employed, together with the $k-\omega$ two-equation turbulence model. The Jameson-Schmidt-Turkel algorithm is used and compared, in terms of accuracy and computational efficiency, with a MUSCL procedure, based upon Roe's flux-difference splitting scheme. Both high and low Reynolds number turbulence models are utilized to represent the sub-layer region. Simulations involving NACA0012 and RAE2822 aerofoils are presented and the results obtained are compared with available experimental data.

INTRODUCTION

Transonic flows are of significant practical importance in the commercial aircraft industry. Due to the presence of subsonic and supersonic regions, shocks and separation zones the numerical simulation of t flow regime is a challenging task. It is well-known that, in the simulation of such flows, the predicted lift and drag are very sensitive to non-physical effects induced by the physical and numerical approximations employed. This means that special care must be taken, in the choice of both the flow algorithm and the turbulence model, if the resulting flow solver is to be useful for the process of aerodynamic design. Currently, a valid approach to simulating practical turbulent flows is the use of the time-averaged Navier-Stokes equations, along with a low-order turbulence model. In this respect, two-equation models appear to satisfy the minimum requirements for a complete model in the sense that they need no extra information about the turbulence structure. Although two-equation models have well-known short-comings, they can produce reasonable results for a range of transonic flow problems. Among the family of two-equation turbulence models, the $k-\omega$ model of Wilcox [1] is attractive in that it produces good results while retaining simplicity of the implementation. The model leads to reasonably accurate predictions for two-dimensional boundary layer flows in the presence of both adverse and favourable pressure gradients. The major weakness of the model is its sensitivity to the free-stream conditions; however, this drawback can be remedied by adding some modifications to the method. Computational efficiency can be increased by employing wall functions in order to represent the flow in the regions immediately adjacent to walls. The use of this approach affects the accuracy of the model and its ability to capture subtle features of the flow, such as separation. Nevertheless, the computations may then be performed on a coarser grid, and the result is a considerable reduction in the computational cost. Numerical dissipation is a crucial ingredient of any compressible flow solver and requires special attention in turbulent flow simulations. Addition of a small amount of dissipation to the flow field can result in major errors, such as delay in separation, which can decrease the lift of an aerofoil drastically. In this work, two different algorithms are considered. The first is the Jameson-Schmidt-Turkel (JST) [2,3] scheme, which involves a blend of fourth-order and second-order dissipations switched by means of a pressure sensor. This scheme is sensitive to the dissipation tuning parameters and the form of the sensor that is employed, and is especially interesting for its computational efficiency. The second method employs the Monotone Upstream-centered Scheme for Conservation Laws (MUSCL) concept, using Roe's flux-difference splitting [4,5] as the basis. The MUSCL scheme has a good record of achievements in the simulation of compressible flows [6] and exhibits a robust and reliable approach. This method has no requirement for tuning parameters, and proves to be fairly insensitive to the type of limiter

1. *Associate Professor, Center of Excellence in Energy Conversion, School of Mechanical Engineering, Sharif University of Technology, Tehran, 11365-3567, Iran.*

which is employed. The choice of various limiters was investigated in a previous 1D study and the limiter used in this paper was proved to be among the best choices [6]. A detailed comparison of various density based schemes can be found elsewhee [3]. In this work, the main goal is to evaluate various combinations of turbulence models and numerical algorithms, with the objective of finding a suitable candidate for the practical 3D flow simulations. The governing equations for compressible turbulent flows are presented, followed by a brief description of both the high and the low Reynolds number $k-\omega$ turbulence models. A general solution approach based upon the Galerkin finite element method on unstructured triangular grids is described and the two solution algorithms used here are outlined. A number of test cases, involving NACA0012 and RAE2822 aerofoils, are solved and the results are compared with experimental data.

GOVERNING EQUATIONS

The equations governing unsteady compressible turbulent flow are derived by introducing the Favre (mass) and conventional time averages into the mass, momentum and energy conservation equations. The mass average is used for the velocity components and the total energy, while the conventional time average is employed for the density and pressure. As a result of the averaging procedure, the governing equations are expressed in terms of mean flow variables. In the $k-\omega$ model, two differential equations, governing the variation of the turbulence kinetic energy k and the turbulence specific dissipation ω , are added. The turbulence viscosity is expressed as a combination of these two variables.

Basic Conservation Equations

The basic system of conservation equations can be expressed, in the non-dimensional conservative form, as:

$$\frac{\partial U}{\partial t}+\frac{\partial F^j}{\partial x_j}-\frac{\partial G^j}{\partial x_j}=S \tag{1}$$

where the summation convention is employed and:

$$U=\begin{bmatrix}\rho\\ \rho u_1\\ \rho u_2\\ \rho E\\ \rho k\\ \rho\omega\end{bmatrix},\qquad F^j=\begin{bmatrix}\rho u_j\\ \rho u_1u_j+p\delta_{1j}\\ \rho u_2u_j+p\delta_{2j}\\ (\rho E+p)u_j\\ \rho k u_j\\ \rho\omega\, u_j\end{bmatrix}$$

$$G^j=\begin{bmatrix}0\\ \tau_{1j}\\ \tau_{2j}\\ u_i\tau_{ij}-q_j+D_{kj}\\ D_{kj}\\ D_{\omega j}\end{bmatrix},\quad S=\begin{bmatrix}0\\ 0\\ 0\\ 0\\ P_k-D_k\\ P_\omega-D_\omega\end{bmatrix} \tag{2}$$

for $i,j=1,2$. Here all the variables are time-averaged mean values and the non-dimensionalization has been based upon the density, velocity, molecular viscosity of the free-stream and a characteristic length of the problem. In the above equations t denotes time, x_i the coordinate relative to a Cartesian coordinate system $O\,x_1\,x_2$, u_i the component of the velocity vector in direction x_i, ρ the density, p the pressure and δ_{ij} the Kronecker delta. The total energy per unit mass is defined as $E=e+u_i\,u_i/2+k$, where e is the mass-averaged specific internal energy and k is the turbulence kinetic energy. The fluid is assumed to be an ideal gas, with constant specific heat ratio γ . The variation of the molecular dynamic viscosity is obtained by the Sutherland's law.

Turbulence Model

In this work, the standard $k-\omega$ turbulence model is used. This is one of the most promising two-equation models in the sense of computational performance. The idea of using the specific dissipation rate, ω dates back to 1942 when Kolmogorov proposed the first two-equation models of turbulence. The quantity ω is regarded as the ratio of the rate of dissipation per unit turbulence kinetic energy. The form of the equation for ω has changed as the $k-\omega$ model has evolved over the past five decades. The standard form of the $k-\omega$ model was presented by Wilcox [1] and later some modifications to the model were devised. The Wilcox's $k-\omega$ model has five closure constants which, like all of the two-equation models, have been introduced in replacing unknown double and triple correlations with algebraic expressions involving known turbulence and mean-flow properties. This model involves solution of two transport equations, as shown in Eqs. (1) and (2), to compute the turbulent viscosity according to $\mu_t=\rho\,k\,\mathrm{Re}\,/\omega$. The stress tensor is given by:

$$\tau_{ij}=\frac{2(\mu+\mu_t)}{\mathrm{Re}}\left(\epsilon_{ij}-\frac{1}{3}\frac{\partial u_k}{\partial x_k}\delta_{ij}\right)-\frac{2}{3}\rho\,k\delta_{ij}$$

$$\text{with }\epsilon_{ij}=\frac{1}{2}\left(\frac{\partial u_i}{\partial x_j}+\frac{\partial u_j}{\partial x_i}\right) \tag{3}$$

In Eq. (2), q_i represents the component of the heat flux vector that contains both the molecular and turbulent contributions, that is, the heat flux in direction x_j is modeled as:

$$q_j=\frac{-1}{\mathrm{Re}}\left(\frac{\mu}{\mathrm{Pr}}+\frac{\mu_t}{\mathrm{Pr}_t}\right)\frac{\partial T}{\partial x_j} \tag{4}$$

where T is temperature and Pr and Pr_t represent the molecular and turbulent Prandtl numbers, respectively. The quantities $D_{k\,j}$ and $D_{\omega\,j}$ contain the effect of both molecular diffusion and turbulent transport and are

modelled as:

$$D_{kj} = \frac{1}{\mathrm{Re}}\left(\mu + \frac{\mu_t}{\sigma_k}\right)\frac{\partial k}{\partial x_j}$$

$$D_{\omega j} = \frac{1}{\mathrm{Re}}\left(\mu + \frac{\mu_t}{\sigma_\omega}\right)\frac{\partial \omega}{\partial x_j} \tag{5}$$

The production and dissipation of k and ω are modeled as:

$$P_k = \tau_{ij}^t \frac{\partial u_i}{\partial x_j}, \quad P_\omega = \frac{\alpha\omega}{k}P_k$$

$$D_k = \beta^*\rho\omega k, \quad D_\omega = \beta\rho\omega^2 \tag{6}$$

In the above equations, the closure constants are:

$$\beta = \frac{3}{40}, \quad \beta^* = 0.09$$

$$\alpha = \frac{5}{9}, \quad \sigma_k = \sigma_\omega = 2 \tag{7}$$

This model can be integrated down to any solid boundary and takes into account the molecular viscous effect in the regions close to a wall, where the molecular viscosity dominates the eddy viscosity. This type of model is known as a low Reynolds number model, in contrast with the high Reynolds number models which cannot simulate the flow in the viscous sublayer region. With high Reynolds number models, wall functions can be employed to represent the solution in this viscous region. The flow field is then only modelled up to a certain distance away from the wall, with the remainder of the flow-field assumed to follow the specific behaviour imposed by the wall function.

FINITE ELEMENT FORMULATION

The starting point for the development of a finite element approximate solution procedure is a variational formulation of the problem. To achieve this, consider a trial function space T and a weighting function space W, which are initially defined to consist of all suitably smooth functions. In addition, all functions in the set T will satisfy the initial condition of the problem. A weak variational formulation of the problem is then: find U in T, satisfying the problem boundary conditions, such that for all W in W and for all $t > t_0$:

$$\int_\Omega \frac{\partial U}{\partial t} W\, d\Omega = \int_\Omega F^j \frac{\partial W}{\partial x_j} d\Omega - \int_\Gamma F^j n_j W\, d\Gamma$$
$$- \int_\Omega G^j \frac{\partial W}{\partial x_j} d\Omega + \int_\Gamma G^j n_j W d\Gamma + \int_\Omega SW d\Omega \tag{8}$$

here, n_j represents the x_i -component of the unit outward normal to boundary Γ. The domain Ω is discretized into a general assembly of linear triangular elements, with the nodes numbered from 1 to p. Subsets T^p and W^p of the trial and weighting function sets T and W are then defined and the standard finite element shape functions are used. An approximate solution to the variational problem can be obtained by the Galerkin method. The integrals appearing in the Galerkin formulation can be evaluated in the standard finite element form by looping over elements and boundary edges and summing individual elements and boundary edge contributions. An alternative approach uses an edge-based data structure for the unstructured mesh [7,8]. The edge-based data structure will be more attractive when the 3D extension is attempted as it can lead to significant reductions in both the CPU time and memory requirements. In terms of the edge-based data structure, the finite element formulation can be written as:

$$\left[M\frac{dU}{dt}\right]_I = -\sum_{s=1}^{m_I} C_{II_S}^j \{(F_I^j + F_{I_S}^j) - (G_I^j + G_{I_S}^j)\}$$
$$+ [M_L]_I S_I + \langle \sum_{f=1}^{2} D_f \{(4\overline{F}_I^n + 2\overline{F}_{J_f}^n + F_I^n - F_{J_f}^n)$$
$$- (4\overline{G}_I^n + 2\overline{G}_{J_f}^n + G_I^n - G_{J_f}^n)\}\rangle_I \tag{9}$$

where the edge s in the mesh joins nodes I and I_s, and J_1 and J_2 are the boundary nodes which are connected to boundary node I. The $C_{II_s}^j$ and D_f are the weight coefficients [6]. The bracketed terms are only non-zero when node I is located on a boundary. The matrix M appearing on the left hand side of the above equation denotes the finite element consistent mass matrix. For the steady flow analysis which is of interest here, this matrix is replaced by the lumped (diagonal) mass matrix M_L, which allows the use of truly explicit time marching procedures.

Numerical Dissipation

There are a variety of methods of achieving stabilization by adding numerical dissipation. Two approaches are followed, which lead to stable schemes with a discontinuity capturing capability, based upon the

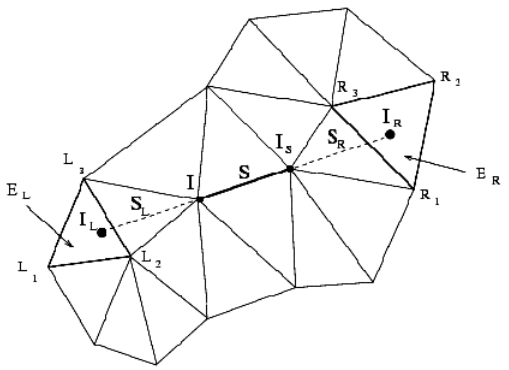

Figure 1. Dummy nodes and corresponding elements.

replacement of the actual flux function in the above equation by a consistent numerical flux function. In this work, two schemes are investigated. The first scheme is a higher-order upwind (MUSCL) algorithm based on the well-known Roe's flux-difference splitting method. In order to implement the method in a FEM methodology, a 1D stencil as shown in Figure 1 is used. The interface values required for the Roe averaging is obtained for each edge II_s . Here a limiter in the form of:

$$I(x,y) = \frac{x(y^2+2\epsilon^2)+y(2x^2+\epsilon^2)}{2x^2-xy+2y^2+3\epsilon^2} \tag{10}$$

is used where ϵ^2 is a small constant. A forward difference approximation is employed to construct the time marching method.

The second method is a popular numerical dissipation method due to Jameson et al [2]. The method is computationally efficient and its implementation is fairly easy. In this method, a three stage Runge-Kutta time stepping scheme in the form of:

$$\begin{cases} U_I^{(0)} = U_I^n \\ U_I^{(k)} = U_I^n - \alpha_k \Delta t\,[M_L](R_I^{(k-1)} - D_I^{(0)}) \quad \text{for } k=1,2,3 \\ U_I^{n+1} = U_I^{(3)} \end{cases} \tag{11}$$

is used to advance the solution from time level $t = t_n$ to time level $t = t_{n+1} = t_n + \Delta t$. Here, $\alpha_1 = 0.6$, $\alpha_2 = 0.6$, $\alpha_3 = 1.0$ and $R_I^{(k-1)}$ is the right hand side of Eq. (9) and D_I is the standard artificial dissipation of Jameson's method:

$$D_I = \sum_{s=1}^{m_I} \frac{12\,\min(\lambda_I,\lambda_{I_s})}{m_I+m_{I_s}} \left(\epsilon_{II_s}^{(2)} \frac{U_{I_s}-U_I}{m_I} - \epsilon_{II_s}^{(4)} \left(\nabla^2 U_{I_s} - \nabla^2 U_I\right)\right) \tag{12}$$

where the second order operator is approximated according to:

$$\nabla^2 U_I \approx \frac{1}{m_I} \sum_{s=1}^{m_I} (U_{I_s} - U_I) \tag{13}$$

Here λ is the maximum eigen-value of the Jacobian matrix $l_j\,\partial F^j/\partial U$ in absolute value, where $l = (l_1, l_2, l_3)$ is the unit vector in the direction of the edge II_S . The parameters $\epsilon_{II_S}^{(2)}$ and $\epsilon_{II_S}^{(3)}$ are defined by:

$$\epsilon_{II_s}^{(2)} = \kappa^{(2)}\,\max(P_I, P_{I_s})$$

$$\epsilon_{II_s}^{(4)} = \max(0, \kappa^{(4)} - \kappa^{(2)}\,\max(P_I, P_{I_s})) \tag{14}$$

Where:

$$P_I = \sum_{s=1}^{m_I} (p_{I_s} - p_I) \,/\, \sum_{s=1}^{m_I} (p_{I_s} + p_I) \tag{15}$$

is the nodal value of a pressure switch.

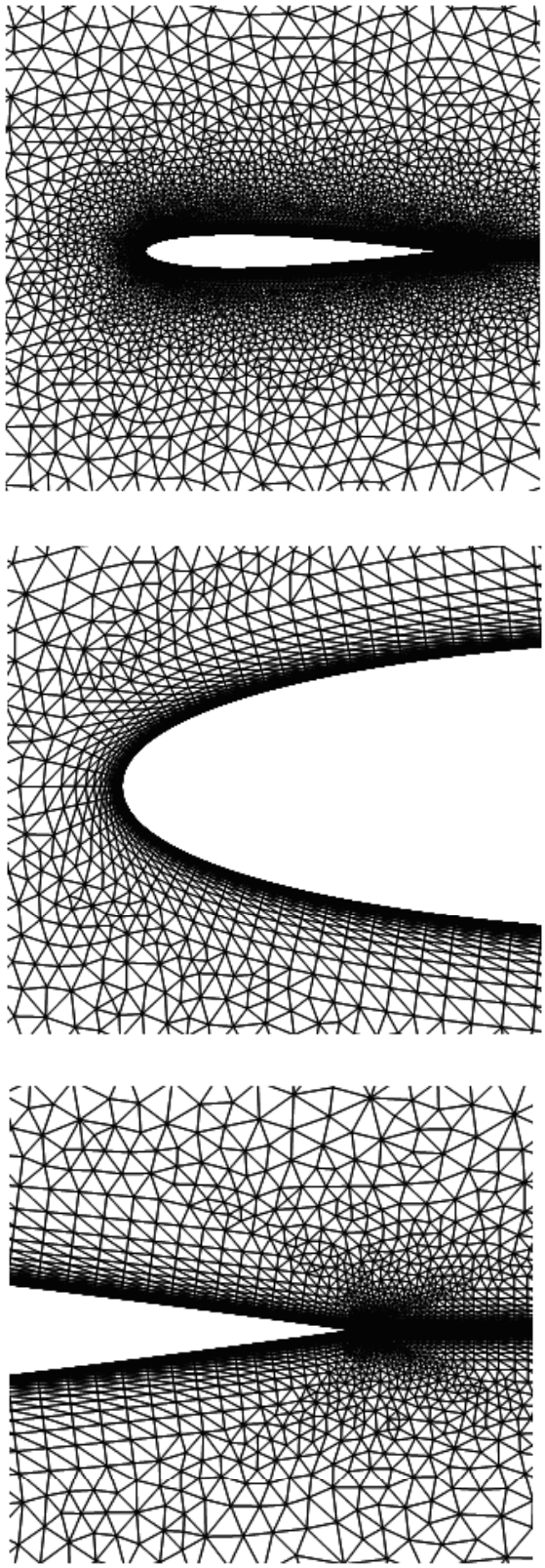

Figure 2. Plots of grid used for NACA0012 aerofoil.

Mesh Generation

The efficient numerical simulation of turbulent flow problems requires the use of meshes involving highly

stretched elements close to the solid boundary. The method used here to generate unstructured meshes involves three separate phases [9]. Firstly, the boundaries of the computational domain are discretised, with the nodal points placed according to a user specified mesh control function. In the second phase, unstructured layers of highly stretched triangular elements are generated adjacent to those boundary surface components which represent solid walls [9]. The height and number of these layers is specified by the user in such a way that the boundary layer profile can be adequately represented. The layers are constructed by generating points, along boundary normals, and then connecting these points to form triangular elements. If normals begin to intersect, the process is locally terminated. Finally, the remainder of the domain is discretised using a Delaunay procedure [10].

NUMERICAL RESULTS

Transonic flows over NACA0012 and RAE2822 aerofoils are studied. The chosen test cases cover a range of flow conditions, involving both shocks and separation zones. The flow conditions for each selected test case are given in Table 1. Both low-Re and high-Re $k-\omega$ models are tested and both MUSCL and JST schemes are employed. The solution is started from free-stream conditions for all cases. To account for the effect of the wind tunnel walls, a corrected angle of attacks have been used for some cases. No correction in Mach number or Reynolds number has been imposed.

The specification of the computational grids employed is given in Table 2. In this table, N_p is the number of nodes, N_e is the number of elements and N_w is the number of nodes on the aerofoil, while δ is the distance of the first layer of grid points from the aerofoil surface. For the NACA0012 aerofoil, three different grids are used: G1, which is suitable for low-Re model computations, and G2 and G3 which are designed for high-Re model computations. The grids G4 and G5 are for the RAE2822 aerofoil and are suitable for low-Re and high-Re calculations respectively. Figures 2 and 3 show plots of grids used for NACA0012 and RAE2822 aerofoils inturn. Table 3 gives information on the computations performed, detailing the grid, the

Table 1. Definition of Test Cases

Test	Airfoil	M	Re	α
A	NACA0012	0.75	3.8E6	2.26
B	NACA0012	0.70	9.0E6	1.49
C	RAE2822	0.73	6.5E6	2.79

Table 2. Specification of Grids

Grid	Airfoil	N_p	N_e	N_w	δ
G1	NACA0012	14097	27939	205	0.00001
G2	NACA0012	9851	19514	168	0.0001
G3	NACA0012	3831	7426	195	0.001
G4	RAE2822	14180	28083	246	0.00001
G5	RAE2822	6838	13399	246	0.0001

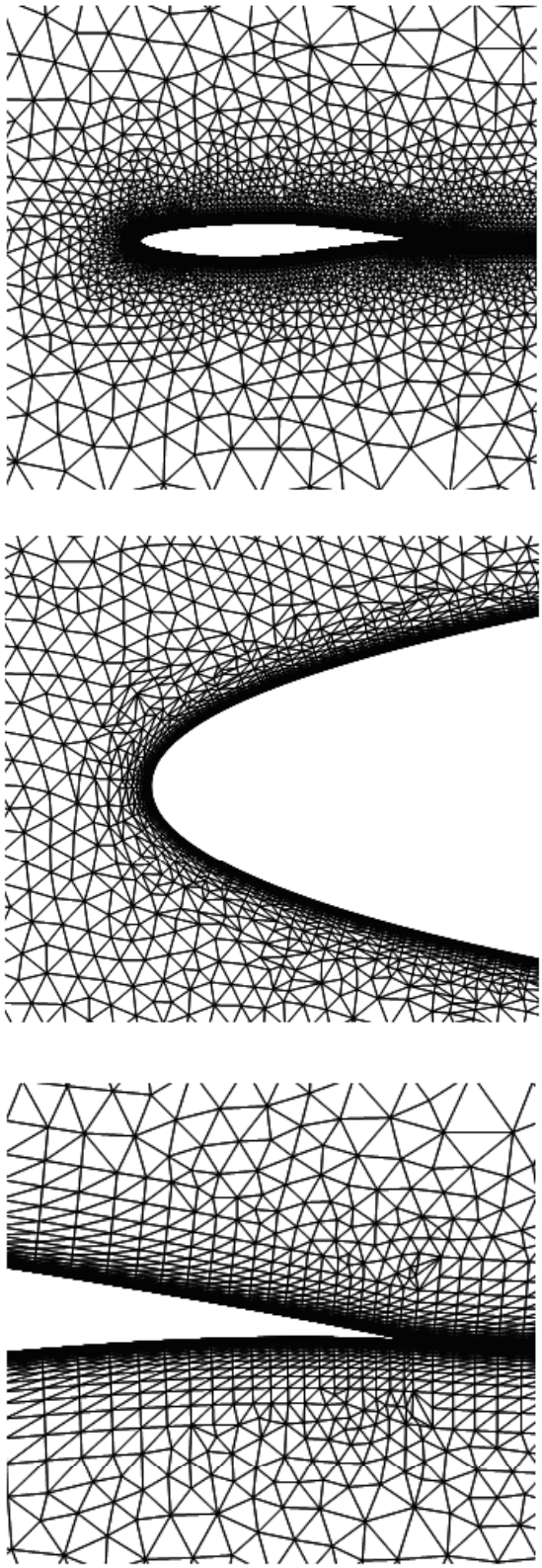

Figure 3. Plots of grid used for RAE2822 aerofoil.

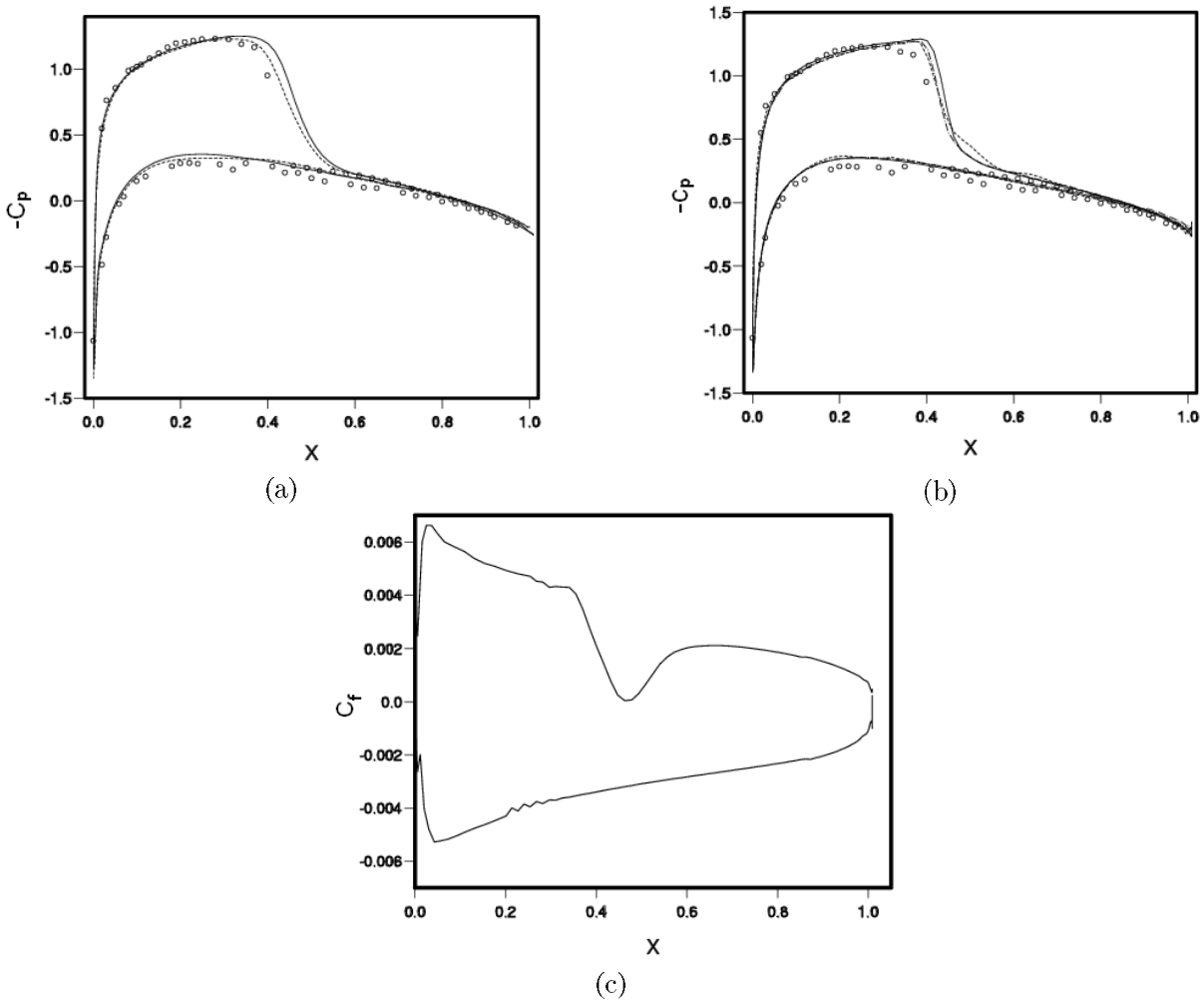

Figure 4. Results obtained for NACA0012 aerofoil (test case A): (a) Pressur coefficient: experiment (circle), Low-Re MUSCL (solid line) and High-Re MUSCL (dashed line), (b) Pressur coefficient: experiment (circle), Low-Re MUSCL (solid line) and High-Re JST with δ=0.0001 (dashed line) and High-Re JST with δ=0.001 (dash-dot lines), (c) Skin friction obtained by Low-Re MUSCL.

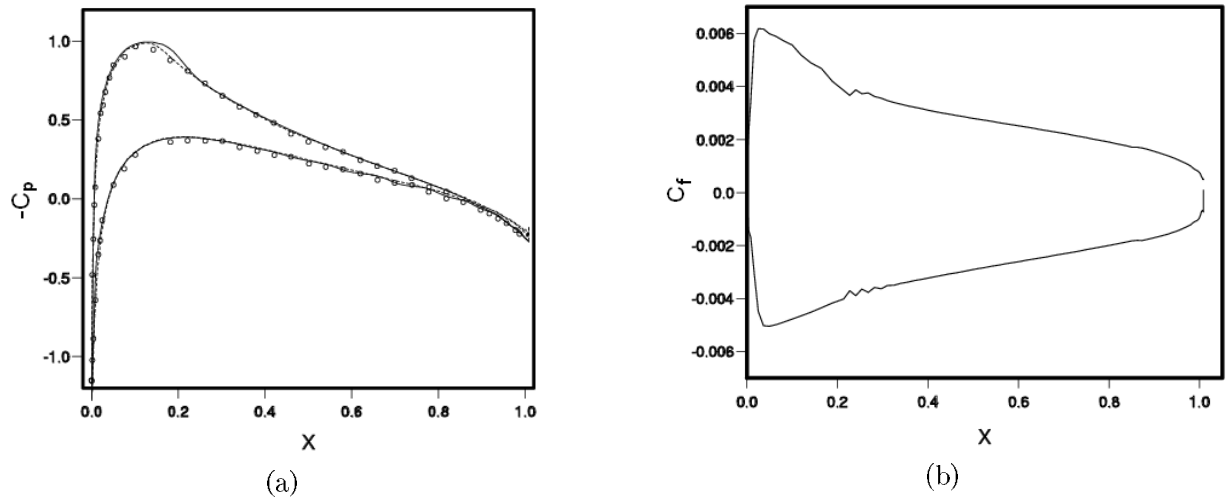

Figure 5. Results obtained for NACA0012 aerofoil (test case B): (a) Pressure coefficient: experiment (circle), Low-Re MUSCL (solid line), High-Re JST (dashed line), (b) Skin friction obtained by Low-Re MUSCL.

turbulence model as well as the solution algorithm employed.

Test Case A

This test case involves a fully attached transonic flow over a NACA0012 aerofoil. Details of the computations performed, designated A1 to A5, are given in Table 3. Figure 4 shows the pressure coefficient distributions obtained with the different combinations of flow algorithm and low/high-Re turbulence model. It is seen that the results are in good agreement with the experimental data [11], with the JST scheme presenting a sharper shock. It is also interesting to note that the coarsening of the grid does not cause a noticeable change in the distribution when wall functions are employed. In Figure 4, the skin friction distribution for A1 is also shown.

Test Case B

A shock free attached transonic flow over a NACA0012 is the solution of the second problem. The flow conditions are given in Table 1. In Figure 5, the computed wall pressure coefficient distributions of B1 and B3 (see Table 3) are compared with experimental observations [11]. The result of computation B2 is indistinguishable from that of B1. The computations are in good agreement with experimental data. This figure also shows the skin friction distributions obtained by B1.

Test Case C

In this test case, an attached transonic flow over a RAE2822 aerofoil is studied. The RAE2822 aerofoil is especially interesting for its shape and curvature. The experimental data for this case is known as Case 9 and is available from [12]. This is a popular test case, and has been investigated by many researchers. Figure 6 shows the distributions of wall pressure coefficient and skin friction obtained by C1, C2 and C3 (Table 3). The overall agreement with experimental data is good, but the low-Re model tends to predict shocks a little upstream of their correct location. The computed skin friction distributions from C1 and C2 are also shown in Figure 6. When wall functions are used, there is a considerable under-prediction of skin friction. For this reason, the skin friction distributions obtained with the high-Re turbulence model are not shown.

Table 3. Specification of Computations

Result	Test	Algorithm	Turbulence Model	Grid
A1	A	MUSCL	Low-Re	G1
A2	A	JST	Low-Re	G1
A3	A	MUSCL	High-Re	G2
A4	A	JST	High-Re	G2
A5	A	JST	High-Re	G3
B1	B	MUSCL	Low-Re	G1
B2	B	JST	Low-Re	G1
B3	B	JST	High-Re	G3
C1	C	MUSCL	Low-Re	G4
C2	C	JST	Low-Re	G4
C3	C	JST	High-Re	G5

CONCLUSIONS

The simulation of transonic turbulent flow over two aerofoil types has been considered. In the search for computationally efficient methods, both the low-Re and the high-Re $k-\omega$ turbulence models were considered, along with the MUSCL and Jameson-Schmidt-Turkel solution schemes. It has been found that the high-Re turbulence model is generally accurate enough to capture the general physics of the flow-field; however, it does not lead to a reliable skin friction

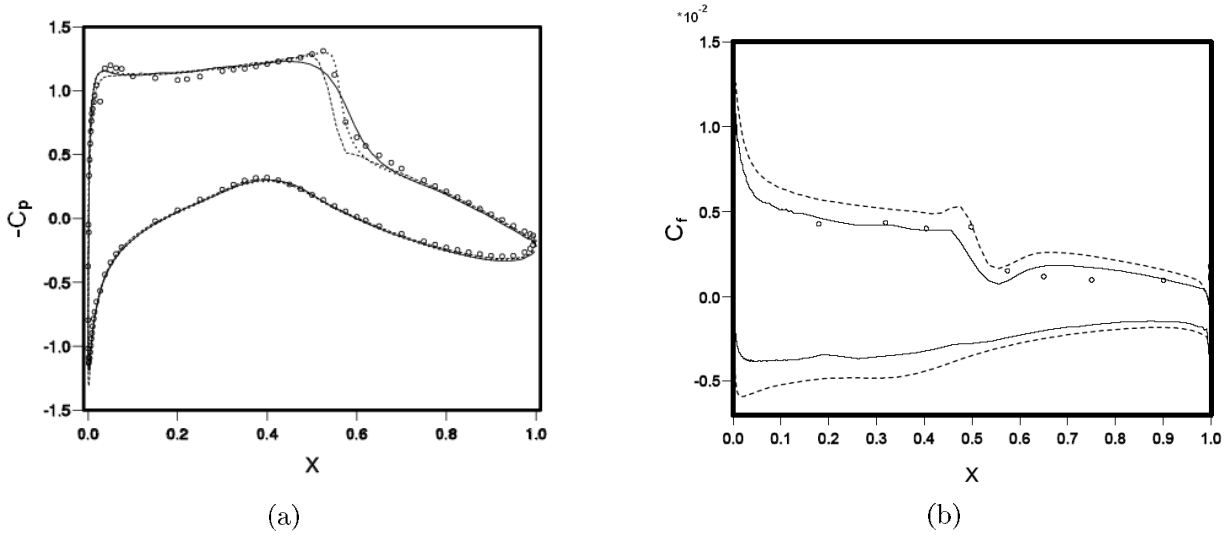

(a) (b)

Figure 6. Results obtained for RAE2822 aerofoil (test case C): (a) Pressure coefficient: experiment (circle) Low-Re MUSCL (solid line), Low-Re JST (dashed line), High-Re JST (dot line), (b) Skin friction: experiment (circle), Low-Re MUSCL (solid line), Low-Re JST (dashed line).

distribution. The low-Re $k-\omega$ model gives fairly accurate skin friction distributions for all the cases attempted in this work.

REFERENCES

1. Wilcox, D.C., "Re-assessment of the scale determining equation for advanced turbulence models", *AIAA J.*, **26**, PP 1299-1310(1988).
2. Jameson, A., Schmidt, W. and Turkel, E., "Numerical simulation of the Euler equations by finite volume method using Runge-Kutta time stepping schemes", *AIAA paper 81-1259* , (1981).
3. Swanson, R.C. and Turkel, E., "On central-difference and upwind schemes", *J. Comp. Physics*, **101**, PP 292-306(1992).
4. Roe, P., "Approximate Riemann solvers, parameter vectors and difference schemes", *J. Comp. Physics*, **43**, PP 357-372(1981).
5. Morrison, J., "Flux-difference split scheme for turbulent transport equations", *AIAA paper 90-5251*, (1990).
6. Manzari, M.T., Lyra, P.R.M., Morgan, K. and Peraire, J., "An unstructured grid FEM/MUSCL algorithm for the compressible Euler equations", *Proceeding of the 8th Intl conf. on FEM in fluids*, Barcelona, Spain, PP 379-388(1993).
7. Peraire, J., Peiro, J. and Morgan, K., "A 3D finite element multigrid solver for the Euler equations", *AIAA paper 92-0449* , (1992).
8. Mavriplis, D.J., "Three dimensional unstructured multigrid for the Euler equations", *AIAA paper 91-1549* , (1991).
9. Hassan, O., Morgan, K., Probert, E.J. and Peraire, J., "Unstructures Tetrahedral Mesh Generation for Three Dimensional Viscous Flows", *Inter. J. Num. Meth. Engg*, **39**, PP 549-567(1996).
10. Weatherill, N.P., "Delaunay triangulation in computational fluid dynamics", *Computer Mathematics and Applications*, **24**, PP 129-150(1992).
11. Harris, C.D., "Two-dimensional aerodynamic charateristics of the NACA0012 airfoil in the Langley 8-foot transonic pressure tunnel", *NASA-TM-81927* , (1981).
12. Cook, P.H., McDonald, M.A. and Firmin, C.P., "Aerofoil RAE2822 pressure distributions and boundary layer and wake measurements", *AGARD*, **138**, (1979).